Journal of Orthopaedic Translation (2018) 15, 91—103

Available online at www.sciencedirect.com

ScienceDirect

journal homepage: http://ees.elsevier.com/jot

PERSPECTIVES

Quantitative analysis of skeletal muscle by computed tomography imaging—State of the art

Klaus Engelke [a,b,*], Oleg Museyko [b], Ling Wang [c], Jean-Denis Laredo [d]

[a] FAU, Department of Medicine 3, University Hospital, Erlangen, Germany
[b] Friedrich-Alexander University Erlangen-Nuremberg, Institute of Medical Physics, Erlangen, Germany
[c] Department of Radiology, Beijing Jishuitan Hospital, Beijing, China
[d] AP-HP, Department of Radiology, Hôpital Lariboisière, Assistance Publique des Hôpitaux de Paris & Université Paris Diderot, Paris, France

Received 17 July 2018; received in revised form 16 October 2018; accepted 19 October 2018
Available online 28 October 2018

KEYWORDS
Adipose tissue;
Computed tomography;
Fat infiltration;
Muscle;
Muscle density

Abstract The radiological assessment of muscle properties—size, mass, density (also termed radiodensity), composition, and adipose tissue infiltration—is fundamental in muscle diseases. More recently, it also became obvious that muscle atrophy, also termed muscle wasting, is caused by or associated with many other diseases or conditions, such as inactivity, malnutrition, chronic obstructive pulmonary disorder, cancer-associated cachexia, diabetes, renal and cardiac failure, and sarcopenia and even potentially with osteoporotic hip fracture. Several techniques have been developed to quantify muscle morphology and function. This review is dedicated to quantitative computed tomography (CT) of skeletal muscle and only includes a brief comparison with magnetic resonance imaging. Strengths and limitations of CT techniques are discussed in detail, including CT scanner calibration, acquisition and reconstruction protocols, and the various quantitative parameters that can be measured with CT, starting from simple volume measures to advanced parameters describing the adipose tissue distribution within muscle. Finally, the use of CT in sarcopenia and cachexia and the relevance of muscle parameters for the assessment of osteoporotic fracture illustrate the application of CT in two emerging areas of medical interest.

* Corresponding author. Department of Medicine 3, University Hospital, Erlangen, Germany.
E-mail address: klaus.engelke@imp.uni-erlangen.de (K. Engelke).

https://doi.org/10.1016/j.jot.2018.10.004

Introduction

The quantitative assessment of muscle properties is of increasing interest in musculoskeletal research and routine. Historically, computed tomography (CT) and magnetic resonance imaging (MRI) have been used in the diagnosis and monitoring of muscle diseases such as myopathies and muscular dystrophies [1–3]. Muscle imaging has also been used to assess muscle atrophy or muscle wasting caused by or associated with inactivity, denervation, fasting, malnutrition, chronic obstructive pulmonary disorder, cancer-associated cachexia, diabetes, renal failure, cardiac failure, Cushing syndrome, sepsis, burns, and trauma [4]. More recently, the paradigm of the bone–muscle unit [5,6] has focussed musculoskeletal research on quantitative muscle assessments such as muscle volume, CT muscle density and content, and distribution of adipose tissue. A new field of application is sarcopenia, where muscle function and perhaps muscle mass are important parameters to measure [7,8].

In skeletal muscle, lipids are either stored as adipocytes, with fat imaging characteristics, either in between muscle groups (perimuscular adipose tissue), or as interstitial (intramuscular) adipose tissue inside muscles (extramyocellular lipids) or as intramyocellular lipid (IMCL) droplets, which are not visually identified as fat in CT or MRI but modify the imaging appearance of muscle tissue [9]. The combination of intramuscular and perimuscular adipose tissue is typically denoted as intermuscular adipose tissue (IMAT) (Figure 1). Increased amounts of intermuscular adipose tissue correlate with cardiovascular risk [10], while the presence of IMCL is a risk factor for of insulin resistance [11]. Increased baseline extramyocellular lipid in isolated supraspinatus muscle tears is associated with surgical repair failure at 6-month follow-up [12].

The two standard techniques available for body composition parameters quantification are dual X-ray absorptiometry (DXA), which provides lean and fat mass assessment, and bioelectrical impedance, which estimates fat-free and fat masses. However, both bioelectrical impedance and DXA cannot provide a spatially resolved distribution of muscle and adipose tissue. This is the domain of CT and MRI. While this review is focussed on CT, a brief comparison between MRI and CT may help the reader to put both techniques into perspective.

MRI provides better soft tissue contrast than CT (Figure 2), but standard spin-echo T1-weighted sequences only provide a qualitative assessment of fat, which appears white, compared with muscle, which in this sequence is dark. The extend of larger agglomerations of adipose tissue can be measured, but the true fat content of muscle cannot be determined from T1-weighted images because the grey values of the muscle voxels do not scale in a known way with the fat content. MR spectroscopy (MRS) and Dixon sequences [13,14] are MR techniques originally developed to quantify the fat content of the liver, which, from the perspective of MRI, is a very homogenous organ. MRS is the only imaging method that allows for a detailed analysis of the acquired MR spectrum and, more specifically, for the separation of intracellular and extracellular lipids [15,16]. However, with MRS, only a very small volume of interest, a so-called spectroscopy voxel with a volume about 1 cm^3, is analysed. This works well for the liver but for muscle, such a small volume may not be representative of the overall fat distribution, especially in elderly and diseased individuals with a high and inhomogeneous muscle fat infiltration. A solution could be a multivoxel MRS protocol [17], but applications in muscle have rarely been reported.

MR Dixon sequences provide a scalable map of the fat fraction from 1 to 100%, in which a grey value of 1 corresponds to a fat fraction of 0.1% and a grey value of 1000 corresponds to a fat fraction of 100%. A quantitative map of the muscle fat fraction can be obtained once the muscle has been segmented. Several variants of Dixon sequences exist. However, accuracy errors of the muscle fat faction may be rather large and depend on the specific implementation on a given scanner. Also, many implementations are dedicated to liver but not to muscle imaging [18,19].

In contrast to MRI, CT is faster, more widely accessible, and cheaper. Radiation exposure of arms or legs is low (<0.5 mSv), while volumetric muscle measurements of the trunk are associated with higher exposure. For example, using a low-dose protocol, exposure for a single slice scan at the height of L3 is about 0.1–0.2 mSv depending on the slice thickness and about 2 mSv for a volumetric scan at the level of L1-4, which is still rather moderate when compared

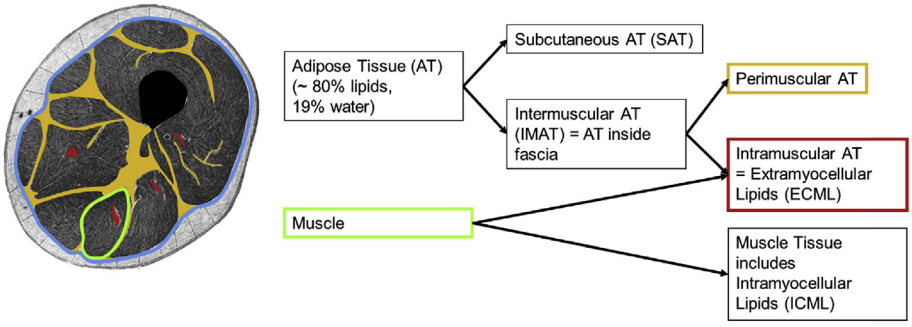

Figure 1 Muscle–lipid system illustrated for the thigh. The blue contour denotes the fascia that separates subcutaneous tissue from the intrafascia region. The green contour outlines a single muscle also denoted as a muscle organ in this contribution to distinguish it from muscle tissue that includes intramyocellular lipids but excludes intramuscular AT (red), which is composed of extramyocellular lipids. Intermuscular AT is the combination of perimuscular AT (yellow) and intramuscular AT (red).
AT = adipose tissue.

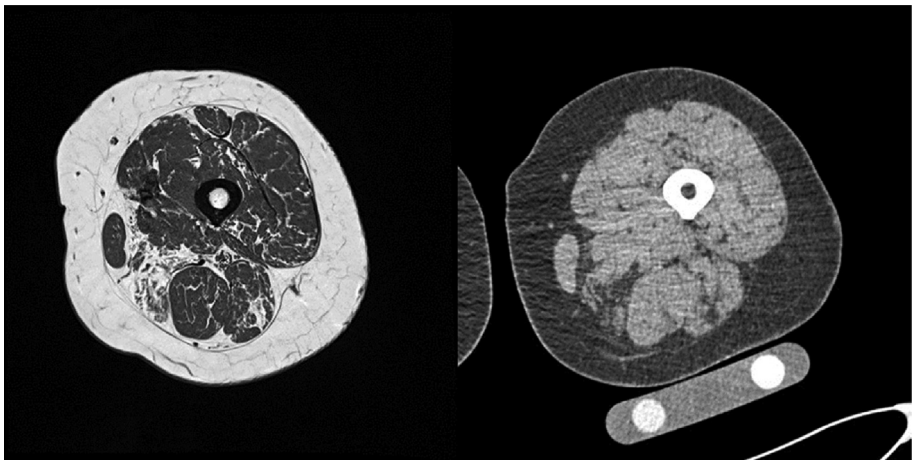

Figure 2 T1-weighted MRI (left) and a low radiation exposure CT (right) image of the thigh. The CT image contains an in-scan calibration phantom to obtain a scan with specific CT values of water. The slice position does not match exactly, and the slice thickness differs.
MRI = magnetic resonance imaging; CT = computed tomography.

with an annual background radiation of about 2.5 mSv. One advantage of CT is the possibility to quantify the muscle density also termed as muscle attenuation or muscle radiation attenuation, which linearly depends on the muscle fat content. The muscle volume may be measured either with MRI or CT. However, the spatial resolution of CT images is higher. Typical MR parameters are a slice thickness of 3 mm and an in-plane pixel size of 0.5 mm, whereas for CT, a slice thickness of 1 mm and an in-plane pixel size of 300 microns are state of the art.

In this contribution, we will first review CT imaging protocols including methods for muscle density calibration and segmentation methods used in quantitative muscle research. An overview of basic and advanced parameters that can be quantified in a CT image and their potential limitations will be given. Finally, the use of muscle parameters in clinical routine and research will be discussed.

Methods of quantitative CT imaging

CT imaging techniques

Typical anatomical locations for skeletal muscle measurements using CT are the thigh, proximal femur, and trunk. CT acquisition and reconstruction parameters vary widely across studies. Most CT muscle studies are performed on whole-body clinical CT scanners. A spiral CT scan or single slices of the targeted volume are acquired. These scanners are widely available, and protocols can easily be tailored to the specific location. Dedicated peripheral CT scanners have been used in some studies to image muscle and adipose tissue of arms or legs [20,21]. As these scanners lack flexibility and scan times are high, this review is restricted to the whole-body equipment.

Although CT studies on muscle assessment appeared not long after the introduction of the first CT scanner in the mid-1970s, little has been published on acquisition protocols for muscle measurements. For the thigh and upper femur, the following settings have been reported: tube voltage of 100—120 kV, exposure: 40—200 mAs, slice thickness 1—10 mm and a soft to medium reconstruction kernel [22—25]. Thicker slices reduce noise and are adequate when the muscle volume or density is of primary interest. For a more advanced analysis of the adipose tissue distribution, a higher spatial resolution is required, and a slice thickness of $\leq$2 mm is preferable. In the thigh and proximal femur, scans usually cover 10—20 cm, but in some studies, the complete upper or lower limb was scanned [26,27], while in others, a single 10-mm-thick slice was acquired at mid-thigh [22,28]. Several studies applied a retrospective analysis of existing CT scans, often initially collected in epidemiological or cross-sectional studies, to measure the bone mineral density (BMD) and assess fracture risk [25,28—30].

Studies dedicated to the assessment of the paraspinal muscles typically assessed the complete lumbar spine, acquiring either a spiral scan or single 3- to 5-mm-thick slices at the level of the intervertebral disks [31—35]. Another application of CT is the evaluation of cachexia in patients with cancer, where the volume of the subcutaneous and visceral fat together with the of the abdominal and paraspinal muscles is measured. For this purpose, analysis is often limited to a single 5- to 10-mm-thick CT slice at the level of L3 [36—39]. In many other instances, existing CT scans from clinical routine are analysed.

Muscle analysis and quantitative parameters

The most straightforward quantitative measurements are the muscle area from a single slice or muscle volume from a stack of slices covering a whole muscle. These measurements require a prior segmentation. However, muscle segmentation is a difficult step, due to the low soft tissue contrast, especially at the trunk where muscles and surrounding organs have similar CT values. Therefore, the most simplistic segmentation approach is a manual outline of the muscles [23,34,40], an acceptable technique as long as the number of slices to be processed is small. The advantage of a manual segmentation is the use of expert knowledge to outline the muscle border, although different

experts will never fully agree on a specific segmentation. However, when a larger stack of CT images needs to be segmented, as with spiral scanning, a more automated segmentation approach is required.

Most of the literature on muscle segmentation is dedicated to MRI, whereas reports using CT are sparse [25,27,41–47]. In several clinical studies and research projects, commercially or publically available software tools such as Slice-O-Matic (http://www.tomovision.com/index.html), OsiriX (http://www.osirix-viewer.com), or ImageJ (https://imagej.nih.gov/ij/) have been used. OsiriX and ImageJ do not provide dedicated muscle segmentation algorithms, but standard segmentation tools such as thresholding, contouring regions, or volumes of similar signal intensity that define muscle, fat, or organs in combination with morphological operations can be easily combined with corrective operator interaction. Three studies [48–50], in which the three software tools were compared, reported excellent agreement between paraspinal muscle of cross-sectional area (CSA) measurements of abdominal and paraspinal muscles, despite the use of a simple threshold or even fully manual segmentation.

In the thigh, usually first the outer margin, i.e., the skin, then the fascia, and finally the individual muscles within the fascia are successively segmented [25]. In the trunk, statistical shape or atlas-based approaches [41,51] have been proposed to facilitate the segmentation of abdominal and paraspinal muscles, which is complicated by the presence of organs and visceral fat. Atlas-based approaches, which require prior training with a gold standard, seem to be the method of choice to separate individual muscles, for example, the quadratus lumborum, multifidus, and sacrospinalis within the paraspinal muscle group. Similar segmentation techniques have been suggested for the hip and thigh muscles [27].

Analysis of entire muscles requires scanning of a large-volume. However, most often, only a small range (several centimetres) of a muscle is scanned to reduce the radiation dose. In this case, area and volume measurements need to be normalized, for example, to the square of the body height [24,39,52,53], to be representative regarding fatty infiltration assessment. The trunk muscle area at the L4-5 level or 5 cm above is highly correlated with the total body skeletal muscle volume ($r^2 > 0.8$) [54]. In the appendicular skeleton, radiation exposure is much lower than that in the trunk and larger volumes can be scanned.

The assessment of the muscle density requires a calibration step but not necessarily muscle segmentation. Representative muscle density values may be obtained by geometrically defined volumes of interest (VOIs) placed in the muscle of interest such as a circle for a slice-based analysis or a sphere or cylinder for a volume-based analysis. A detailed overview of studies in which a geometrical VOI was used to determine the muscle density has been provided in Ref. [55]. So far, in the vast majority of studies measuring the muscle density, muscle was first segmented and the muscle area was obtained as a primary outcome.

It must be understood that the muscle density is not a physical density measured in mg/cm^3, but a 'CT density' measured in Hounsfield units. The term muscle attenuation is used synonymously [56], but the term CT density will be used in the present contribution. By default, each CT scanner is calibrated to water:

$$\text{CT number} = \frac{\mu - \mu_w}{\mu_w} \cdot 1000[\text{HU}]$$

where μ is the linear absorption coefficient of the material under investigation, and μ_w is the attenuation coefficient of distilled water at room temperature. In a calibrated scanner, the CT numbers for water and air are 0 and -1000, respectively. For water-equivalent materials, i.e., for materials with comparable mass absorption coefficients such as muscle, CT values quantify percentage density differences to water. A CT value of 1 HU quantifies a density difference to water of 0.1%. The physical density of skeletal muscle, including IMCLs, is about 1.055 g/cm^3 [57–59] compared with 1 g/cm^3 for water. Thus, for a properly calibrated scanner, the CT value of skeletal muscle also termed as muscle tissue is about 50–60 HU. Published values of IMCL content in human skeletal muscle as measured by MRS are between 6% and 14% [60] compared with 2%–9% for chemical analysis [57] and 2%–5% for histochemical analysis [61]. Additional infiltration of extracellular lipids—or adipose tissue within muscle—will decrease the muscle density value below 50 HU.

Owing to CT scanner instabilities, the water value often deviates from 0 HU. Figure 3 shows CT values measured in the European Spine Phantom (ESP), which was scanned on 41 scanner units. The ESP is a reference standard used in bone densitometry, in which soft tissue is made of a water-equivalent plastic. Each scan was acquired with the same phantom on a different CT scanner, and 17 different CT scanner models from four manufacturers were tested. All scanners were regularly calibrated according to the local hospital and manufacturer standard operating procedures. In the ESP, a cylindrical VOI positioned in the water-equivalent soft tissue region anterior to the vertebrae was analysed. In 15% of the scanner units (6 of 41), CT values differed by 5 or more HU from 0. In the thigh, a difference of 5 HU in the water value causes a 15% difference in the muscle density [25]. Thus, for accurate muscle density measurements the use of a calibration phantom should be considered. This phantom can either be scanned with the subject (simultaneous calibration). An example is

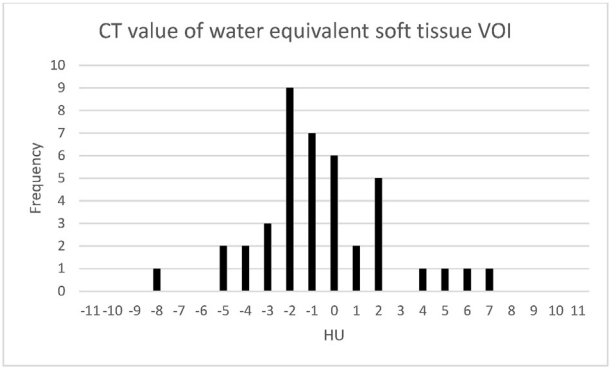

Figure 3 CT values of the water-equivalent soft tissue material of the same European Spine Phantom measured anteriorly to the vertebrae from 41 different CT scanners.
CT = computed tomography.

shown in Figure 2. Alternatively the phantom can be scanned before or after the patient (asynchronous calibration).

CT values are used not only to determine the muscle density but also to segment muscle and adipose tissue. Furthermore, they play a central role in estimating the adipose tissue content within muscle. Table 1 lists the published CT values used for these three different applications and the terminology used in the corresponding reference for muscle and adipose tissue parameters. It shows that even for a given application, for example, to determine the tissue composition, CT values vary significantly, which has also been noted in an earlier review [55]. One source of confusion in comparing CT values of muscle and adipose tissue among previous works is the great variability in terminology. For example, the term muscle is typically used to denote the organ muscle, which includes adipose tissue, whereas the term muscle tissue includes intramyocellular lipids (ICML) but excludes adipose tissue. Thus, the CT value of muscle will vary considerably depending on its adipose tissue content. Some authors, however, use muscle tissue synonymously with muscle [24]. CT values for muscle tissue are higher than those of muscle.

Table 1 CT values used for segmentation, tissue composition, and the measurement of adipose tissue infiltration of muscle.

Reference	Terminology	CT value (HU)	Comment
Segmentation			
Mitsiopoulos 1998 [109]	Skeletal muscle	−29 to 150	
Mitsiopoulos 1998 [109], Irving 2007 [49], Mühlberg 2017 [25]	Adipose tissue	−190 to −30	
Lönn 1994 [67]	Adipose tissue	−190 to −30	
	Muscle incl. skin/visceral organs	−29 to 151	
Fuchs 2018 [110]	Muscle density	−29 to 150	
Edmunds 2016 [26]	Fat	−200 to 10	
	LDM	−9 to 40	
	NDM	41 to 70	
Van der Werf 2018 [24]	Muscle tissue	−29 to 150	
Neander 1997 [111]	Muscle	10 to 100	
Strandberg 2010 [22]	Muscle	1 to 101	
Tissue composition			
Goodpaster 2000 [101]	Skeletal muscle	0 to 100	
Margadant 2016 [38]	Muscle tissue	60	
Mourtzakis 2008 [39]	Skeletal muscle	−29 to 150	
	Subcutaneous and intramuscular adipose tissue	−190 to −30	
	Visceral adipose tissue	−150 to −50	
Heymsfield 1997 [112]	Adipose tissue	−90 to −30	
	Nonadipose tissue lean	−29 to 151	
Muscle fat infiltration			
Goodpaster 2000 [101]	LDM	0 to 29	
	NDM	30 to 100	
Lang 2008 [29], Frank-Wilson 2018 [62]	Fat, lean		HU thresholds to separate lean and fat mass derived from in-scan calibration phantom
Gargiulo 2014 [113]	Fat	−200 to −6	
	Loose connective tissue	−5 to 20	
	LDM	20 to 40	
	Normal muscle	40 to 200	
Daguet 2011 [23]	Pure fat	−108	Internal calibration − . fat
	Pure muscle	60	Internal calibration − psoas muscle of young healthy individuals
Mühlberg 2017 [25]	Pure adipose tissue	≈ −100	Internal calibration − thigh subcut. adipose tissue
	HDM	35	Internal calibration − psoas muscle of young healthy individuals
Hahn 2016 [106]	Muscle	30 to 80	
	Fat	−190 to −30	

HDM = high-density muscle; LDM = low-density muscle; NDM = normal-density muscle; subcut. = subcutaneous.
The CT value range from −29 to 150 originally used by Mitsiopoulos and even earlier by Lönn has been used in many subsequent studies as can be seen in the table.

Pure muscle and high-density muscle have been used to denote the muscle density in young healthy individuals [23,25], although it can be speculated that some amount of intermuscular and intramuscular adipose tissue is present even in young healthy individuals, and therefore, that the term pure muscle may not be fully appropriate. However, the average muscle density of young people may serve as an upper fix point for muscle density calibration using CT. The terminology is even more diverse for fat/adipose tissue.

Differences in CT values shown in Table 1 are probably not very relevant when used as thresholds for segmentation of muscle, subcutaneous, or visceral compartments. Automated techniques may use fixed thresholds to initiate the segmentation but are usually refined without using absolute thresholds. In semiautomatic procedures, initial threshold-based contours guide the operator and are corrected if required. In contrast to segmentation, differences in CT values have a much larger impact on the quantification of the adipose tissue content within a single muscle or within a muscle group contained by the perimuscular deep fascia such as the paraspinal muscles or the whole thigh muscles. Such an entity is often analysed as a whole to avoid a rather difficult segmentation of individual muscles. Therefore, the separation of intermuscular and intramuscular adipose tissue components is of interest. Obviously, the use of absolute thresholds is problematic. They are not consistent across the literature (Table 1) and do not take into account deviations from the ideal water calibration of the CT scanner. Therefore, some studies have suggested techniques based on in-scan calibration phantoms [29,62], internal calibration [23], or both [25].

For a more detailed characterisation of the adipose tissue infiltration, a frequency analysis (Figure 4) of the density values [23,55] and of its spatial distribution has been suggested [25]. Based on the histogram of the CT values of the segmented muscle, five different bins were distinguished [23]: pure muscle, pure fat and voxels containing 25%, 50%, and 75% adipose tissue according to the muscle density, respectively. This is the quantitative analogue to the Goutallier score [63] used to qualitatively score fatty muscle degeneration.

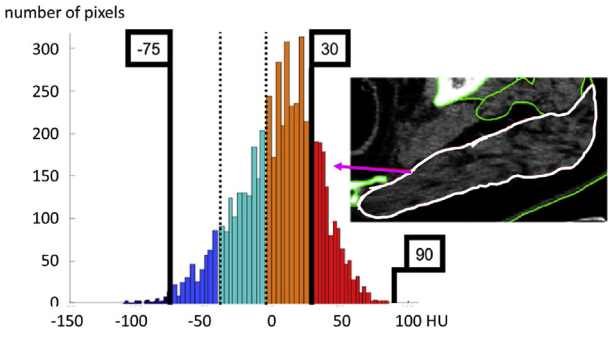

Figure 4 Histogram of density values on a CT slice of the left glutaeus maximus muscle (inset). Red pixels, with a density between 130 and 190 Hounsfield units (HU), were classified as pure muscle. Deep navy blue pixels, with a density of $\leq$75 HU, were classified as pure fat. Between the −75 and 130 HU boundaries, brown pixels were counted as being composed of 75% muscle and 25% fat, blue–green pixels as 50% muscle and 50% fat, and medium blue pixels as 25% muscle and 75% fat (Figure 2 from Ref. [23]). The adipose tissue content of the individual voxels of the glutaeus maximus is not presented in colour.
CT = computed tomography.

The histogram analysis requires two values, one for pure adipose tissue and one for pure muscle. In Ref. [25], the value for adipose tissue was obtained by internal calibration based on the distribution of subcutaneous adipose tissue corrected for potential inclusion of water, oedema, and vessels. The value for pure muscle was obtained from a group of young active athletes. For each CT scan, this high-density muscle value was individually corrected for potential water calibration offsets using an in-scan calibration phantom [25]. If the CT scanner is stable, the in-scan calibration phantom can be replaced by asynchronous calibration, which means that phantom and subject scans are typically not performed at the same time [64].

A further step is the quantification of the spatial distribution of adipose tissue infiltration and the characterisation of muscle structures termed as washed out or moth eaten (Figure 5) in radiological scoring systems [65]. For this purpose, we have recently used a number of different descriptors that quantify the texture [25]. They can either be applied to the CT images directly or after image binarisation. While details are beyond the scope of this review, Figure 7 illustrates the principle, assuming four different muscle–fat compositions, where for simplicity, muscle in red has a value of 1 and fat in white has a value of 0, corresponding to a binary image. Texture parameters may help to better distinguish different structural patterns than CT density (or in case of the simplified simulation, relative volume).

Muscle mass in gram is not a primary parameter of CT. It has been estimated by multiplying the muscle volume by a density of 1.06 g/cm^3 [66,67] or 1.04 [68]. Accuracy of this approach is questionable as the degree of muscle fat infiltration is neglected. A better approach would be to calculate the physical density of each voxel from its CT number, which as described previously, denotes the percentage density difference from water. Nevertheless, correlation coefficients of $r^2 \geq 0.96$ have been reported in healthy volunteers [68,69] between muscle mass in the thigh estimated by CT, even with the simplified technique, and fat-free mass (FFM) measured by DXA. Correlation between the muscle area measured by CT and FFM was $r^2 = 0.74$. Another study of premenopausal lean and obese women reported correlations between the CT muscle area and DXA FFM at the thigh of $r^2 = 0.59$ and $r^2 = 0.58$, respectively [70].

Applications of quantitative muscle imaging by CT

Several recent systematic reviews and meta-analyses impressively demonstrated that muscle imaging by quantitative CT plays an important role in a large variety of diseases affecting organs such as the lung [71], liver [72,73], or abdomen [74,75]. Further systematic reviews were dedicated to muscle characteristics in cerebral palsy [76], vascular claudication [77], low back pain [78], and muscle

Mercuri Score	
Stage 0	normal appearance
Stage 1	early moth-eaten appearance, with scattered small areas of decreased CT density
Stage 2a	late moth-eaten appearance, with numerous discrete areas of decreased CT density (CT) with beginning confluence, comprising less than 30% of the volume of the individual muscle
Stage 2b	late moth-eaten appearance, with numerous discrete areas of decreased CT density (CT) with beginning confluence, comprising less 30% - 60% of the volume of the individual muscle
Stage 3	washed-out appearance, fuzzy appearance due to confluent areas of decreased CT density with muscle still present at the periphery
Stage 4	end-stage appearance, muscle replaced by lower CT density, connective tissue and fat, with only a rim of fascia and neurovascular structures distinguishable

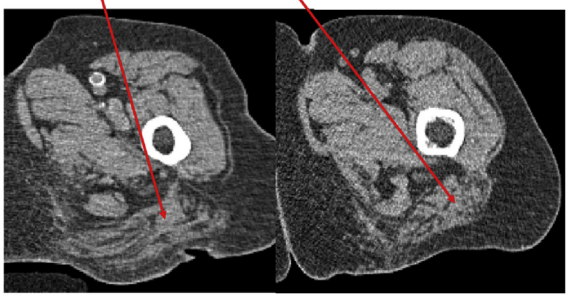

Figure 5 The Mercuri score for grading the muscle appearance in neuromuscular diseases [65] and two CT images demonstrating moth-eaten and washed-out muscle structures.
CT = computed tomography.

fatigue in old age [79]. CT imaging is used to assess muscle diseases, age-related muscle deterioration (sarcopenia) and muscle wasting (cachexia), other chronic diseases associated with or causing muscle weakness, after organ transplantation specifically and surgery in general; in body composition studies to assess efficacy of exercise or nutritional intervention; and to predict the risk of osteoporotic fracture or the impact of fracture on muscle. Obviously, it is beyond the scope of this review to cover all these applications in relevant details, in particular, as other imaging techniques—radiography, MRI, and DXA—are often used as well. Therefore, the following two sections have been selected as example applications.

Sarcopenia and cachexia

"Cachexia and sarcopenia present several analogies in both the pathogenic mechanisms and the clinical picture. The loss of muscle mass and strength is a hallmark of these two clinical conditions. Although frequently overlapping and often indistinguishable, especially in old individuals, these two conditions should be considered as distinct clinical entities" [80]. The first definition of sarcopenia proposed in 1988 [81] was completely based on appendicular lean mass, determined from a whole-body DXA scan. Later definitions of sarcopenia included impaired muscle strength and/or physical performance [82—85]. None of these definitions is based on CT, although specific thresholds of the muscle size assessed by CT have been proposed for the diagnosis of sarcopenia [86]. Yet, the controversy on which imaging modality should be preferred is still ongoing [87,88]. One limitation to the use of CT is its lower degree of standardisation when compared with DXA, but also controversies concerning which of the muscle parameters assessed by CT should be used. DXA only provides lean mass, and in sarcopenia research, more studies used DXA than CT. Similarly to the use of DXA for routine BMD measurements, DXA may be preferred for sarcopenia in daily clinical routine. However, CT and MRI provide some muscle measurements, such as fatty infiltration, an important factor of muscle degeneration, which are not available for DXA and are key techniques to address the pathophysiology of sarcopenia and mechanisms of interventions. Several epidemiological studies such as Osteoporotic Fractures in Men, AGES-Reykjavik, and Health, Aging, and Body Composition (Health ABC) included CT of the proximal femur and upper shaft, a valuable source for sarcopenia research largely unexplored so far. Also existing CT scans obtained for other diagnostic purposes may be retrospectively analysed to obtain muscle characteristics [89—91].

Cachexia has been defined as "a complex metabolic syndrome associated with underlying illness and characterised by the loss of muscle mass with or without the loss of fat mass". A quick search for cachexia and cancer in PubMed resulted in 1250 entries. The prominent feature of cachexia is "weight loss in adults" [92]. In addition, a more specific definition has been agreed on for cancer cachexia [93]. For patients with cancer, CT imaging is a key diagnosis tool for follow-up diagnosis and treatment monitoring [39]. The potential for opportunistic muscle imaging in such patients has already been emphasised a decade ago [36]. A typical imaging technique in cancer cachexia is the analysis of a single CT at the level of L3. In addition to the muscle volume, density and intramuscular adipose tissue, the volume of subcutaneous and visceral fat volume is determined (Figure 6). However, longitudinal measurements of visceral fat on a single slice are problematic because of motion, in particular that affecting the visceral organs, which can significantly change the local amount of visceral fat.

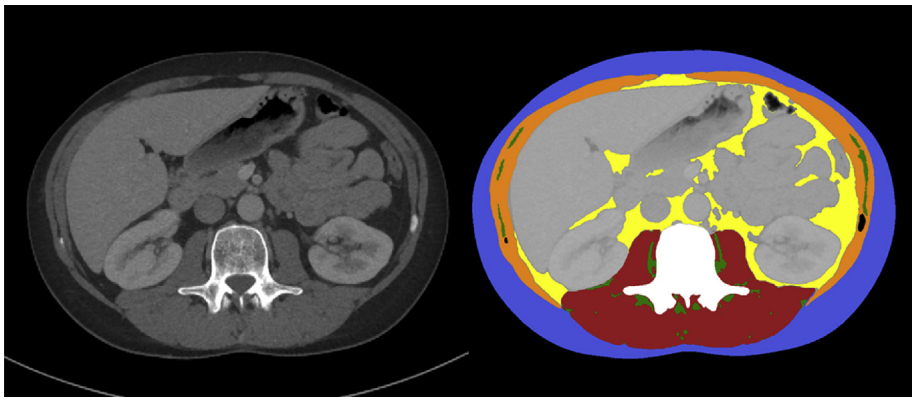

Figure 6 The left CT image at the level of L3; the right segmentation: subcutaneous adipose tissue (blue), paraspinal muscle (brown), abdominal muscle (orange), intramuscular adipose tissue (green), visceral fat (yellow), and visceral organs (grey). CT = computed tomography.

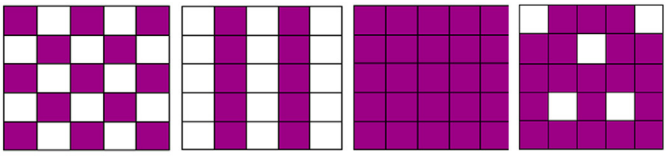

relative volume [%] (**)	50	40	100	80
local inhomogeneity [pixel]	1	0.35	0	0.33
area/volume [edge/pixel]	4$	2.4*	0.8*	1.6*
variogram slope [1/pixel]	0	-0.01	0	-0.014

Figure 7 Four simulated binary muscle (red)—fat (white) distributions where muscle has a value of 1 and fat, of 0. The table shows the results of three different texture parameters plus relative volume. It shows that, for example, the relative volume differs only slightly between the two leftmost structures, while local inhomogeneity discriminates much better. By default, a periodic continuation of the 5 × 5 pattern was assumed for calculations except when marked with an asterisk (*), where zero boundary conditions were used, i.e., all pixels outside the pattern were white; values marked ($) appeared independent of the boundary type used.

Osteoporotic fracture

BMD is an important risk factor for osteoporotic fracture, but the prediction of osteoporotic fracture remains challenging [94]. In particular, progress remains limited for the prediction whether an individual will sustain a hip fracture within the next 5 or 10 years. In contrast to vertebral fractures, almost all osteoporotic hip fractures are caused by a fall, which is associated with muscle strength [95—98]. Age-related loss of skeletal muscle mass is associated with the loss of bone mass [99,100], and low muscle attenuation is associated with obesity and impaired muscle function [101]. So far, only a few studies have investigated the impact of soft tissue parameters on hip fracture. In the Health ABC study, decreases in DXA-derived subcutaneous fat thickness significantly increased hip fracture risk after adjustment for hip areal BMD (aBMD) in men [hazard ratio (HR) 1.44 confidence interval (CI; 1.02—2.02)] and women [HR 1.39 (CI 1.07; 1.82)]. An increase in appendicular lean mass in the leg decreased hip fracture risk in men (HR 0.65 [CI 0.46; 0.92)] but not in women, even after adjustment for the body height [102]. The association between lean mass and fracture was confirmed in the Framingham (leg lean mass) [103], Epidémiologie de l'Ostéoporose (whole-body lean mass) [104], and (WHI; appendicular lean mass) [105] studies, all of which included women only. After adjustment for hip aBMD, fat mass did not significantly increase hip fracture risk in the Epidémiologie de l'Ostéoporose (whole-body fat mass) and WHI (appendicular fat mass) studies. It was not separately assessed in the Framingham study.

In contrast, CT studies showed a significant contribution of muscle characteristics to hip fracture risk. In the pelvis [29], the CSA of total fat and of the extensor and adductor muscles, as well as CT attenuation of the adductor muscles remained significantly lower in fractured individuals after adjustment for age and body mass index. Compared with DXA aBMD alone, fracture discrimination was improved by the inclusion of the soft tissue descriptors in a multivariate model. In the Health ABC study [28], CT attenuation of the thigh muscle predicted hip fracture with a relative risk (RR) of 1.6, which remained significant with an RR of 1.4 after adjustment for aBMD. The RR for aBMD alone was not reported in this study.

In the Osteoporotic Fractures in Men study, composite descriptors combining the stress strain index or bending strength of bone with the muscle CSA were determined by peripheral QCT (pQCT) of the lower limb. These descriptors

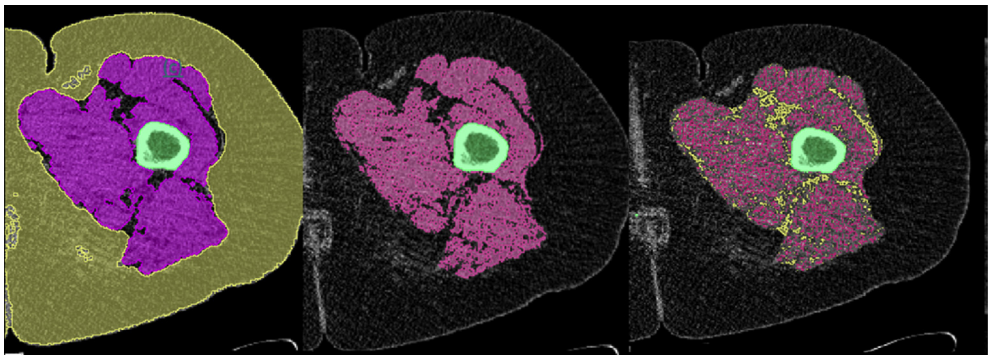

Figure 8 The CT image of the thigh from an elderly individual of the EFFECT study. Left: segmented fascia separating subcutaneous adipose tissue (yellow), muscle (red), and perimuscular adipose tissue (uncoloured); center: muscle tissue; and right: distribution of high-density muscle (red) and intermuscular and intramuscular adipose tissue (yellow). Uncoloured voxels contain mixtures of muscle and adipose tissue.
CT = computed tomography; EFFECT = European Femur Fracture Study.

predicted hip fracture with a hazard ratio (HR) of up to 1.6 that remained significant after adjustment for aBMD of the spine and total hip (HR up to 1.2) [30], but areal total hip BMD alone resulted in an HR of 2.1 for hip fracture prediction. The other two studies [106,107] did not specifically target hip fracture prediction or discrimination.

In the retrospective analysis of the European Femur Fracture Study, the relative volume of adipose tissue in the upper thigh and 12 soft tissue texture parameters characterising the muscle–lipid distribution (Figure 8) were significant discriminators of femur fracture. After combination with the standard BMD in a multivariate model, four parameters remained significant discriminators: BMD and cortical thickness representing the bone strength and the relative volume of adipose tissue representing mechanical protection against the hip fracture by a larger cushion and the surface density of the adipocyte distribution within muscle representing muscle degeneration [108]. Area under the curve values was 0.85 for a combined soft tissue model, 0.84 for a combined bone model containing BMD and cortical thickness, and 0.92 for a model combining soft tissue and bone parameters, indicating that soft tissue parameters discriminated proximal femur fracture and BMD and that a combined approach was providing the best discrimination (Figure 9).

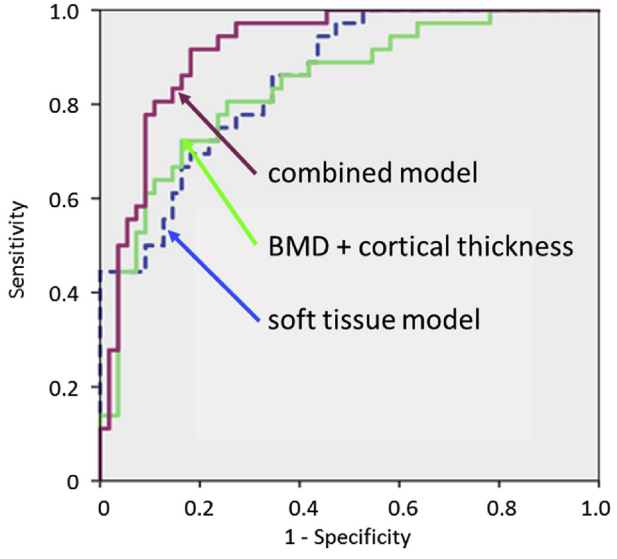

Figure 9 ROC curves of three different models used for hip fracture discrimination of the EFFECT study [108].
BMD = bone mineral density; EFFECT = European Femur Fracture Study. ROC = receiver operator characteristics.

Future directions

Quantitative CT to assess the muscle volume and density is an established technique used routinely in a large variety of applications. Automated or at least semiautomatic segmentation algorithms must be further developed, in particular to analyse larger body parts instead of single slices. The assumption of a well calibrated scanner, i.e., a CT value of zero for water, is misleading and can lead to larger accuracy errors in the determination of the CT muscle density. The use of phantoms should be considered. Standardisation of the terminology is also required.

The analysis of the muscle lipid distribution which is still in its infancy may give new insights into the pathophysiology of sarcopenia and cachexia and could in particular improve risk prediction of osteoporotic hip fracture because it takes into account to some extent the risk of falls through the muscle status. In sarcopenia, CT should be regarded as a complementary imaging method to DXA that in combination with MRI may also improve our understanding on intervention and may better explain effects on functional muscle outcomes than simple lean mass measurements.

Funding

None.

Conflict of interest

None declared.

Appendix A. Supplementary data

Supplementary data to this article can be found online at https://doi.org/10.1016/j.jot.2018.10.004.

References

[1] Burakiewicz J, Sinclair CDJ, Fischer D, Walter GA, Kan HE, Hollingsworth KG. Quantifying fat replacement of muscle by quantitative MRI in muscular dystrophy. J Neurol 2017; 264(10):2053—67.

[2] Ten Dam L, van der Kooi AJ, Verhamme C, Wattjes MP, de Visser M. Muscle imaging in inherited and acquired muscle diseases. Eur J Neurol 2016;23(4):688—703.

[3] Weber A. Magnetic resonance imaging of skeletal musculature. In: Reiser M, Hricak H, Knauth M, editors. Medical radiology — diagnostic imaging. Heidelberg: Springer; 2014.

[4] Cohen S, Nathan JA, Goldberg AL. Muscle wasting in disease: molecular mechanisms and promising therapies. Nat Rev Drug Discov 2015;14(1):58—74.

[5] Frost HM. Muscle, bone, and the Utah paradigm: a 1999 overview. Med Sci Sports Exerc 2000;32(5):911—7.

[6] Frost HM, Schonau E. The "muscle-bone unit" in children and adolescents: a 2000 overview. J Pediatr Endocrinol Metab 2000;13(6):571—90.

[7] Sergi G, Trevisan C, Veronese N, Lucato P, Manzato E. Imaging of sarcopenia. Eur J Radiol 2016;85(8):1519—24.

[8] Boutin RD, Yao L, Canter RJ, Lenchik L. Sarcopenia: current concepts and imaging implications. Am J Roentgenol 2015; 205(3):W255—66.

[9] Wronska A, Kmiec Z. Structural and biochemical characteristics of various white adipose tissue depots. Acta Physiol 2012;205(2):194—208.

[10] Yim JE, Heshka S, Albu J, Heymsfield S, Kuznia P, Harris T, et al. Intermuscular adipose tissue rivals visceral adipose tissue in independent associations with cardiovascular risk. Int J Obes 2007;31(9):1400—5.

[11] Perreault L, Bergman BC, Hunerdosse DM, Eckel RH. Altered intramuscular lipid metabolism relates to diminished insulin action in men, but not women, in progression to diabetes. Obesity 2010;18(11):2093—100.

[12] Lansdown DA, Lee S, Sam C, Krug R, Feeley BT, Ma CB. A prospective, quantitative evaluation of fatty infiltration before and after rotator cuff repair. Orthop J Sports Med 2017;5(7). 2325967117718537.

[13] Dixon WT. Simple proton spectroscopic imaging. Radiology 1984;153(1):189—94.

[14] Pineda N, Sharma P, Xu Q, Hu X, Vos M, Martin DR. Measurement of hepatic lipid: high-speed T2-corrected multiecho acquisition at 1H MR spectroscopy — a rapid and accurate technique. Radiology 2009;252(2):568—76.

[15] Boesch C, Slotboom J, Hoppeler H, Kreis R. In vivo determination of intra-myocellular lipids in human muscle by means of localized 1H-MR-spectroscopy. Magn Reson Med 1997;37(4):484—93.

[16] Velan SS, Durst C, Lemieux SK, Raylman RR, Sridhar R, Spencer RG, et al. Investigation of muscle lipid metabolism by localized one- and two-dimensional MRS techniques using a clinical 3T MRI/MRS scanner. J Magn Reson Imaging 2007; 25(1):192—9.

[17] Forbes SC, Lott DJ, Finkel RS, Senesac C, Byrne BJ, Sweeney HL, et al. MRI/MRS evaluation of a female carrier of Duchenne muscular dystrophy. Neuromuscul Disord 2012; 22(Suppl. 2):S111—21.

[18] Grimm A, Meyer H, Nickel MD, Nittka M, Raithel E, Chaudry O, et al. Evaluation of 2-point, 3-point, and 6-point Dixon magnetic resonance imaging with flexible echo timing for muscle fat quantification. Eur J Radiol 2018;103:57—64.

[19] Grimm A, Meyer H, Nickel MD, Nittka M, Raithel E, Chaudry O, et al. Online A comparison between 6-point Dixon MRI and MR spectroscopy to quantify muscle fat in the thigh of subjects with sarcopenia. JFA; 2018.

[20] Sherk VD, Thiebaud RS, Chen Z, Karabulut M, Kim SJ, Bemben DA. Associations between pQCT-based fat and muscle area and density and DXA-based total and leg soft tissue mass in healthy women and men. J Musculoskelet Neuronal Interact 2014;14(4):411—7.

[21] Erlandson MC, Lorbergs AL, Mathur S, Cheung AM. Muscle analysis using pQCT, DXA and MRI. Eur J Radiol 2016;85(8): 1505—11.

[22] Strandberg S, Wretling ML, Wredmark T, Shalabi A. Reliability of computed tomography measurements in assessment of thigh muscle cross-sectional area and attenuation. BMC Med Imaging 2010;10:18.

[23] Daguet E, Jolivet E, Bousson V, Boutron C, Dahmen N, Bergot C, et al. Fat content of hip muscles: an anteroposterior gradient. J Bone Joint Surg Am 2011;93(20): 1897—905.

[24] van der Werf A, Langius JAE, de van der Schueren MAE, Nurmohamed SA, van der Pant K, Blauwhoff-Buskermolen S, et al. Percentiles for skeletal muscle index, area and radiation attenuation based on computed tomography imaging in a healthy Caucasian population. Eur J Clin Nutr 2018;72(2): 288—96.

[25] Muhlberg A, Museyko O, Laredo JD, Engelke K. A reproducible semi-automatic method to quantify the muscle-lipid distribution in clinical 3D CT images of the thigh. PLoS One 2017; 12(4):e0175174.

[26] Edmunds KJ, Gislason MK, Arnadottir ID, Marcante A, Piccione F, Gargiulo P. Quantitative computed tomography and image analysis for advanced muscle assessment. Eur J Transl Myol 2016;26(2):6015.

[27] Yokota F, Otake Y, Takao M, Ogawa T, Okada T, Sugano N, et al. Automated muscle segmentation from CT images of the hip and thigh using a hierarchical multi-atlas method. Int J Comput Assist Radiol Surg 2018 Jul;13(7):977—86.

[28] Lang T, Cauley JA, Tylavsky F, Bauer D, Cummings S, Harris TB, et al. Computed tomographic measurements of thigh muscle cross-sectional area and attenuation coefficient predict hip fracture: the health, aging, and body composition study. J Bone Miner Res 2010;25(3):513—9.

[29] Lang T, Koyama A, Li C, Li J, Lu Y, Saeed I, et al. Pelvic body composition measurements by quantitative computed tomography: association with recent hip fracture. Bone 2008; 42(4):798—805.

[30] Wong AK, Cawthon PM, Peters KW, Cummings SR, Gordon CL, Sheu Y, et al., Osteoporotic Fractures in Men Research G. Bone-muscle indices as risk factors for fractures in men: the Osteoporotic Fractures in Men (MrOS) study. J Musculoskelet Neuronal Interact 2014;14(3):246—54.

[31] Anderson DE, Bean JF, Holt NE, Keel JC, Bouxsein ML. Computed tomography-based muscle attenuation and electrical impedance myography as indicators of trunk muscle strength independent of muscle size in older adults. Am J Phys Med Rehabil 2014;93(7):553—61.

[32] Hyun SJ, Bae CW, Lee SH, Rhim SC. Fatty degeneration of the paraspinal muscle in patients with degenerative lumbar kyphosis: a new evaluation method of quantitative digital analysis using MRI and CT scan. Clin Spine Surg 2016;29(10): 441—7.

[33] Lee SH, Park SW, Kim YB, Nam TK, Lee YS. The fatty degeneration of lumbar paraspinal muscles on computed tomography scan according to age and disc level. Spine J 2017;17(1):81—7.

[34] Keller A, Gunderson R, Reikeras O, Brox JI. Reliability of computed tomography measurements of paraspinal muscle cross-sectional area and density in patients with chronic low back pain. Spine 2003;28(13):1455—60.
[35] Hu ZJ, He J, Zhao FD, Fang XQ, Zhou LN, Fan SW. An assessment of the intra- and inter-reliability of the lumbar paraspinal muscle parameters using CT scan and magnetic resonance imaging. Spine 2011;36(13):E868—74.
[36] Prado CM, Birdsell LA, Baracos VE. The emerging role of computerized tomography in assessing cancer cachexia. Curr Opin Support Palliat Care 2009;3(4):269—75.
[37] Martin L, Birdsell L, Macdonald N, Reiman T, Clandinin MT, McCargar LJ, et al. Cancer cachexia in the age of obesity: skeletal muscle depletion is a powerful prognostic factor, independent of body mass index. J Clin Oncol 2013;31(12): 1539—47.
[38] Margadant CC, Bruns ER, Sloothaak DA, van Duijvendijk P, van Raamt AF, van der Zaag HJ, et al. Lower muscle density is associated with major postoperative complications in older patients after surgery for colorectal cancer. Eur J Surg Oncol 2016;42(11):1654—9.
[39] Mourtzakis M, Prado CM, Lieffers JR, Reiman T, McCargar LJ, Baracos VE. A practical and precise approach to quantification of body composition in cancer patients using computed tomography images acquired during routine care. Appl Physiol Nutr Metab 2008;33(5):997—1006.
[40] Takahashi N, Sugimoto M, Psutka SP, Chen B, Moynagh MR, Carter RE. Validation study of a new semi-automated software program for CT body composition analysis. Abdom Radiol 2017;42(9):2369—75.
[41] Kamiya N, Zhou X, Chen H, Muramatsu C, Hara T, Yokoyama R, et al. Automated segmentation of recuts abdominis muscle using shape model in X-ray CT images. Conf Proc IEEE Eng Med Biol Soc 2011;2011:7993—6.
[42] Valenzuela W, Ferguson SJ, Ignasiak D, Diserens G, Vermathen P, Boesch C, et al. Correction tool for active shape model based lumbar muscle segmentation. Conf Proc IEEE Eng Med Biol Soc 2015;2015:3033—6.
[43] Popuri K, Cobzas D, Esfandiari N, Baracos V, Jagersand M. Body composition assessment in axial CT images using FEM-based automatic segmentation of skeletal muscle. IEEE Trans Med Imaging 2016;35(2):512—20.
[44] Lee H, Troschel FM, Tajmir S, Fuchs G, Mario J, Fintelmann FJ, et al. Pixel-level deep segmentation: artificial intelligence quantifies muscle on computed tomography for body morphometric analysis. J Digit Imaging 2017;30(4): 487—98.
[45] Kamiya N, Zhou X, Chen H, Muramatsu C, Hara T, Yokoyama R, et al. Automated segmentation of psoas major muscle in X-ray CT images by use of a shape model: preliminary study. Radiol Phys Technol 2012;5(1):5—14.
[46] Chung HC, Cobzas D, Birdsell L, Lieffers J, Baracos V. Automated segmentation of muscle and adipose tissue on CT images for human body composition analysis. In: Miga MI, Won CH, editors. Medical imaging 2009: visualization, image-guided procedures, and modeling, vol. 7261. SPIE Proceedings; 2009.
[47] Wei Y, Xu B, Ying M, Qu J, Duke R. Two dimensional paraspinal muscle segmentation in CT images. In: International Conference on Progress in Informatics and Computing. IEEE; 2017. p. 143—7.
[48] Fortin M, Battie MC. Quantitative paraspinal muscle measurements: inter-software reliability and agreement using OsiriX and ImageJ. Phys Ther 2012;92(6):853—64.
[49] Irving BA, Weltman JY, Brock DW, Davis CK, Gaesser GA, Weltman A. NIH ImageJ and Slice-O-Matic computed tomography imaging software to quantify soft tissue. Obesity 2007; 15(2):370—6.
[50] van Vugt JL, Levolger S, Gharbharan A, Koek M, Niessen WJ, Burger JW, et al. A comparative study of software programmes for cross-sectional skeletal muscle and adipose tissue measurements on abdominal computed tomography scans of rectal cancer patients. J Cachexia Sarcopenia Muscle 2017;8(2):285—97.
[51] Engstrom CM, Fripp J, Jurcak V, Walker DG, Salvado O, Crozier S. Segmentation of the quadratus lumborum muscle using statistical shape modeling. J Magn Reson Imaging 2011; 33(6):1422—9.
[52] Joglekar S, Asghar A, Mott SL, Johnson BE, Button AM, Clark E, et al. Sarcopenia is an independent predictor of complications following pancreatectomy for adenocarcinoma. J Surg Oncol 2015;111(6):771—5.
[53] Kasahara R, Kawahara T, Ohtake S, Saitoh Y, Tsutsumi S, Teranishi JI, et al. A low psoas muscle index before treatment can predict a poorer prognosis in advanced bladder cancer patients who receive gemcitabine and nedaplatin therapy. Biomed Res Int 2017;2017:7981549.
[54] Shen W, Punyanitya M, Wang Z, Gallagher D, St-Onge MP, Albu J, et al. Total body skeletal muscle and adipose tissue volumes: estimation from a single abdominal cross-sectional image. J Appl Physiol (1985) 2004;97(6):2333—8.
[55] Aubrey J, Esfandiari N, Baracos VE, Buteau FA, Frenette J, Putman CT, et al. Measurement of skeletal muscle radiation attenuation and basis of its biological variation. Acta Physiol 2014;210(3):489—97.
[56] Goodpaster BH, Carlson CL, Visser M, Kelley DE, Scherzinger A, Harris TB, et al. Attenuation of skeletal muscle and strength in the elderly: the health ABC study. J Appl Physiol (1985) 2001;90(6):2157—65.
[57] ICRP 1975 Publication 23. Report of the task group on reference man. International commission on radiological protection. Oxford: Pergamon Press; 1975.
[58] Urbancheka MG, Pickenb EB, Kalliainenc lK, Kuzon WM. Specific force deficit in skeletal muscles of old rats is partially, explained by the existence of denervated muscle fibers. J Gerontol Series A Biol Sci Med Sci 2001;56(5):B191—7.
[59] Ward SR, Lieber RL. Density and hydration of fresh and fixed human skeletal muscle. J Biomech 2005;38(11):2317—20.
[60] Schrauwen-Hinderling VB, Hesselink MK, Schrauwen P, Kooi ME. Intramyocellular lipid content in human skeletal muscle. Obesity 2006;14(3):357—67.
[61] Malenfant P, Joanisse DR, Theriault R, Goodpaster BH, Kelley DE, Simoneau JA. Fat content in individual muscle fibers of lean and obese subjects. Int J Obes Relat Metab Disord 2001;25(9):1316—21.
[62] Frank-Wilson AW, Chalhoub D, Figueiredo P, Jonsson PV, Siggeirsdottir K, Sigurdsson S, et al. Associations of quadriceps torque properties with muscle size, attenuation, and intra-muscular adipose tissue in older adults. J Gerontol A Biol Sci Med Sci 2018 Jun 14;73(7):931—8.
[63] Goutallier D, Postel JM, Bernageau J, Lavau L, Voisin MC. Fatty muscle degeneration in cuff ruptures. Pre- and postoperative evaluation by CT scan. Clin Orthop Relat Res 1994; 304:78—83.
[64] Engelke K, Lang T, Khosla S, Qin L, Zysset P, Leslie WD, et al. Clinical use of quantitative computed tomography-based advanced techniques in the management of osteoporosis in adults: the 2015 ISCD official positions-part III. J Clin Densitom 2015;18(3):393—407.
[65] Mercuri E, Talim B, Moghadaszadeh B, Petit N, Brockington M, Counsell S, et al. Clinical and imaging findings in six cases of congenital muscular dystrophy with rigid spine syndrome linked to chromosome 1p (RSMD1). Neuromuscul Disord 2002; 12(7—8):631—8.
[66] Chowdhury B, Sjostrom L, Alpsten M, Kostanty J, Kvist H, Lofgren R. A multicompartment body composition technique

based on computerized tomography. Int J Obes Relat Metab Disord 1994;18(4):219—34.
[67] Lonn L, Kvist H, Ernest I, Sjostrom L. Changes in body composition and adipose tissue distribution after treatment of women with Cushing's syndrome. Metabolism 1994;43(12): 1517—22.
[68] Visser M, Fuerst T, Lang T, Salamone L, Harris TB. Validity of fan-beam dual-energy X-ray absorptiometry for measuring fat-free mass and leg muscle mass. Health, aging, and body composition study-dual-energy X-ray absorptiometry and body composition working group. J Appl Physiol (1985) 1999; 87(4):1513—20.
[69] Levine JA, Abboud L, Barry M, Reed JE, Sheedy PF, Jensen MD. Measuring leg muscle and fat mass in humans: comparison of CT and dual-energy X-ray absorptiometry. J Appl Physiol (1985) 2000;88(2):452—6.
[70] Bredella MA, Ghomi RH, Thomas BJ, Torriani M, Brick DJ, Gerweck AV, et al. Comparison of DXA and CT in the assessment of body composition in premenopausal women with obesity and anorexia nervosa. Obesity 2010;18(11): 2227—33.
[71] Rozenberg D, Martelli V, Vieira L, Orchanian-Cheff A, Keshwani N, Singer LG, et al. Utilization of non-invasive imaging tools for assessment of peripheral skeletal muscle size and composition in chronic lung disease: a systematic review. Respir Med 2017;131:125—34.
[72] van Vugt JL, Levolger S, de Bruin RW, van Rosmalen J, Metselaar HJ, IJzermans JN. Systematic review and meta-analysis of the impact of computed tomography-assessed skeletal muscle mass on outcome in patients awaiting or undergoing liver transplantation. Am J Transplant 2016; 16(8):2277—92.
[73] Chang KV, Chen JD, Wu WT, Huang KC, Hsu CT, Han DS. Association between loss of skeletal muscle mass and mortality and tumor recurrence in hepatocellular carcinoma: a systematic review and meta-analysis. Liver Cancer 2018;7(1):90—103.
[74] Gibson DJ, Burden ST, Strauss BJ, Todd C, Lal S. The role of computed tomography in evaluating body composition and the influence of reduced muscle mass on clinical outcome in abdominal malignancy: a systematic review. Eur J Clin Nutr 2015;69(10):1079—86.
[75] Hasselager R, Gogenur I. Core muscle size assessed by perioperative abdominal CT scan is related to mortality, postoperative complications, and hospitalization after major abdominal surgery: a systematic review. Langenbecks Arch Surg 2014;399(3):287—95.
[76] Barrett RS, Lichtwark GA. Gross muscle morphology and structure in spastic cerebral palsy: a systematic review. Dev Med Child Neurol 2010;52(9):794—804.
[77] Harwood AE, King S, Totty J, Smith GE, Vanicek N, Chetter IC. A systematic review of muscle morphology and function in intermittent claudication. J Vasc Surg 2017;66(4):1241—57.
[78] Suri P, Fry AL, Gellhorn AC. Do muscle characteristics on lumbar spine magnetic resonance imaging or computed tomography predict future low back pain, physical function, or performance? A systematic review. PM R 2015;7(12): 1269—81.
[79] Christie A, Snook EM, Kent-Braun JA. Systematic review and meta-analysis of skeletal muscle fatigue in old age. Med Sci Sports Exerc 2011;43(4):568—77.
[80] Muscaritoli M, Lucia S, Molfino A, Cederholm T, Rossi Fanelli F. Muscle atrophy in aging and chronic diseases: is it sarcopenia or cachexia? Intern Emerg Med 2013;8(7):553—60.
[81] Baumgartner RN, Koehler KM, Gallagher D, Romero L, Heymsfield SB, Ross RR, et al. Epidemiology of sarcopenia among the elderly in New Mexico (Abstract). Am J Epidemiol 1998;147(8):755—63.
[82] Cruz-Jentoft AJ, Baeyens JP, Bauer JM, Boirie Y, Cederholm T, Landi F, et al., European Working Group on Sarcopenia in Older P. Sarcopenia: European consensus on definition and diagnosis: report of the European working group on sarcopenia in older people. Age Ageing 2010;39(4): 412—23.
[83] Fielding RA, Vellas B, Evans WJ, Bhasin S, Morley JE, Newman AB, et al. Sarcopenia: an undiagnosed condition in older adults. Current consensus definition: prevalence, etiology, and consequences. International working group on sarcopenia. J Am Med Dir Assoc 2011;12(4):249—56.
[84] Studenski SA, Peters KW, Alley DE, Cawthon PM, McLean RR, Harris TB, et al. The FNIH sarcopenia project: rationale, study description, conference recommendations, and final estimates. J Gerontol A Biol Sci Med Sci 2014;69(5):547—58.
[85] Dawson-Hughes B, Bischoff-Ferrari H. Considerations concerning the definition of sarcopenia. Osteoporos Int 2016; 27(11):3139—44.
[86] Kim JS, Kim WY, Park HK, Kim MC, Jung W, Ko BS. Simple age specific cutoff value for sarcopenia evaluated by computed tomography. Ann Nutr Metab 2017;71(3—4):157—63.
[87] Buckinx F, Landi F, Cesari M, Fielding RA, Visser M, Engelke K, et al. Pitfalls in the measurement of muscle mass: a need for a reference standard. J Cachexia Sarcopenia Muscle 2018; 9(2):269—78.
[88] Scafoglieri A, Clarys JP. Dual energy X-ray absorptiometry: gold standard for muscle mass? J Cachexia Sarcopenia Muscle 2018 Aug;9(4):786—7.
[89] Nemec U, Heidinger B, Sokas C, Chu L, Eisenberg RL. Diagnosing sarcopenia on thoracic computed tomography: quantitative assessment of skeletal muscle mass in patients undergoing transcatheter aortic valve replacement. Acad Radiol 2017;24(9):1154—61.
[90] Murray TE, Williams D, Lee MJ. Osteoporosis, obesity, and sarcopenia on abdominal CT: a review of epidemiology, diagnostic criteria, and management strategies for the reporting radiologist. Abdom Radiol 2017;42(9):2376—86.
[91] Tamandl D, Paireder M, Asari R, Baltzer PA, Schoppmann SF, Ba-Ssalamah A. Markers of sarcopenia quantified by computed tomography predict adverse long-term outcome in patients with resected oesophageal or gastro-oesophageal junction cancer. Eur Radiol 2016;26(5):1359—67.
[92] Evans WJ, Morley JE, Argiles J, Bales C, Baracos V, Guttridge D, et al. Cachexia: a new definition. Clin Nutr 2008;27(6):793—9.
[93] Fearon K, Strasser F, Anker SD, Bosaeus I, Bruera E, Fainsinger RL, et al. Definition and classification of cancer cachexia: an international consensus. Lancet Oncol 2011; 12(5):489—95.
[94] Rubin KH, Friis-Holmberg T, Hermann AP, Abrahamsen B, Brixen K. Risk assessment tools to identify women with increased risk of osteoporotic fracture: complexity or simplicity? A systematic review. J Bone Miner Res 2013;28(8):1701—17.
[95] Reis P, Moro A, Bins Ely V, Fernandes C, Vilagra J, Peres L, et al. Universal design and accessibility: an approach of the influence of muscle strength loss in the risk of falls in the elderly. Work 2012;41(Suppl. 1):374—9.
[96] Wang X, Ma Y, Wang J, Han P, Dong R, Kang L, et al. Mobility and muscle strength together are more strongly correlated with falls in suburb-dwelling older Chinese. Sci Rep 2016;6: 25420.
[97] Wickham C, Cooper C, Margetts BM, Barker DJ. Muscle strength, activity, housing and the risk of falls in elderly people. Age Ageing 1989;18(1):47—51.
[98] Tinetti ME, Doucette J, Claus E, Marottoli R. Risk factors for serious injury during falls by older persons in the community. J Am Geriatr Soc 1995;43(11):1214—21.

[99] Proctor DN, Melton LJ, Khosla S, Crowson CS, O'Connor MK, Riggs BL. Relative influence of physical activity, muscle mass and strength on bone density. Osteoporos Int 2000;11(11):944—52.
[100] Khosla S, Atkinson EJ, Riggs BL, Melton 3rd LJ. Relationship between body composition and bone mass in women. J Bone Miner Res 1996;11(6):857—63.
[101] Goodpaster BH, Thaete FL, Kelley DE. Composition of skeletal muscle evaluated with computed tomography. Ann N Y Acad Sci 2000;904:18—24.
[102] Malkov S, Cawthon PM, Peters KW, Cauley JA, Murphy RA, Visser M, et al. Hip fractures risk in older men and women associated with DXA-derived measures of thigh subcutaneous fat thickness, cross-sectional muscle area, and muscle density. J Bone Miner Res 2015;30(8):1414—21.
[103] McLean RR, Kiel DP, Berry SD, Broe KE, Zhang X, Cupples LA, et al. Lower lean mass measured by dual-energy X-ray absorptiometry (DXA) is not associated with increased risk of hip fracture in women: the Framingham osteoporosis study. Calcif Tissue Int 2018;103(1):16—23.
[104] Schott AM, Cormier C, Hans D, Favier F, Hausherr E, Dargent-Molina P, et al. How hip and whole-body bone mineral density predict hip fracture in elderly women: the EPIDOS prospective study. Osteoporos Int 1998;8(3):247—54.
[105] Zaslavsky O, Li W, Going S, Datta M, Snetselaar L, Zelber-Sagi S. Association between body composition and hip fractures in older women with physical frailty. Geriatr Gerontol Int 2017;17(6):898—904.
[106] Hahn MH, Won YY. Bone mineral density and fatty degeneration of thigh muscles measured by computed tomography in hip fracture patients. J Bone Metab 2016;23(4):215—21.
[107] Wong AK, Beattie KA, Min KK, Gordon C, Pickard L, Papaioannou A, et al. Peripheral quantitative computed tomography-derived muscle density and peripheral magnetic resonance imaging-derived muscle adiposity: precision and associations with fragility fractures in women. J Musculoskelet Neuronal Interact 2014;14(4):401—10.
[108] Muhlberg A, Museyko O, Bousson V, Pottecher P, Laredo JD, Engelke K. Muscle and adipose tissue characteristics of the thigh discriminate hip fracture as well as BMD. Radiology 2018. in press.
[109] Mitsiopoulos N, Baumgartner RN, Heymsfield SB, Lyons W, Gallagher D, Ross R. Cadaver validation of skeletal muscle measurement by magnetic resonance imaging and computerized tomography. J Appl Physiol (1985) 1998;85(1):115—22.
[110] Fuchs G, Chretien YR, Mario J, Do S, Eikermann M, Liu B, et al. Quantifying the effect of slice thickness, intravenous contrast and tube current on muscle segmentation: implications for body composition analysis. Eur Radiol 2018;28(6):2455—63.
[111] Neander G, Adolphson P, Hedstrom M, von Sivers K, Dahlborn M, Dalen N. Decrease in bone mineral density and muscle mass after femoral neck fracture. A quantitative computed tomography study in 25 patients. Acta Orthop Scand 1997;68(5):451—5.
[112] Heymsfield SB, Wang Z, Baumgartner RN, Ross R. Human body composition: advances in models and methods. Annu Rev Nutr 1997;17:527—58.
[113] Gargiulo P, Helgason T, Ramon C, Johnson Jr H, Carraro U. CT and MRI assessment and characterization using segmentation and 3D modeling techniques: applications to muscle, bone and brain. Eur J Transl Myol 2014;24(1):3298.